

A simple model of the resistive wall mode in tokamaks

Richard Fitzpatrick^{a)}

Institute for Fusion Studies, Department of Physics, University of Texas at Austin, Austin, Texas 78712

(Received 13 February 2002; accepted 19 March 2002)

A simple set of evolution equations is derived for the resistive wall mode in a large aspect-ratio, rotating, viscous, tokamak plasma. The equations take into account the nonlinear deceleration of the plasma rotation generated by mode interaction with both the resistive wall and a static error field. Furthermore, the equations are largely able to explain resistive wall mode data recently obtained from the DIII-D tokamak [*Plasma Physics and Controlled Nuclear Fusion Research* (International Atomic Energy Agency, Vienna, 1986), p. 159]. In particular, the role of the error field in triggering plasma deceleration is elucidated. © 2002 American Institute of Physics.
[DOI: 10.1063/1.1491254]

I. INTRODUCTION

The economic attractiveness of the promising “advanced tokamak” (AT) concept^{1,2} is a strongly increasing function of the normalized plasma pressure, β .³ Now, the maximum achievable β in AT devices is limited by pressure gradient driven, ideal external-kink modes.⁴ Indeed, AT designs are only advantageous if the external-kink β limit is raised substantially due to the presence of a close fitting, *perfectly conducting* wall surrounding the plasma. Unfortunately, all realizable conducting walls possess non-negligible resistivity. According to conventional theory, when a tokamak plasma is surrounded by a close fitting, *resistive* wall, the relatively fast growing ideal external-kink mode is converted into the far more slowly growing “resistive wall mode” (RWM). The latter mode grows on the characteristic L/R time of the wall, τ_w , and has virtually identical stability boundaries to those of the external-kink mode in the complete absence of a wall.⁵ Now, τ_w is long compared to most plasma timescales, but still generally much shorter than the duration of the plasma discharge. Hence, all attractive advanced tokamak designs are predicated on the assumption that the RWM can somehow be stabilized.

Experimentally, it is found that tokamak plasmas can exceed the no-wall β limit (i.e., the ideal β limit calculated in the complete absence of a wall) for time periods much longer than τ_w , provided that the plasma is rotating sufficiently rapidly.^{6–8} This suggests that the RWM can somehow be stabilized via plasma *rotation*. A plausible stabilization mechanism was first discovered numerically by Bondeson and Ward,⁹ and later accounted for analytically by Betti and Freidberg.¹⁰ According to this mechanism, stabilization of the RWM is a combined effect of plasma *rotational inertia* and *dissipation* due to interaction with the sound wave continuum at a toroidally coupled resonant surface lying within the plasma. It was subsequently discovered that neoclassical effects significantly weaken sound wave dissipation, while simultaneously enhancing dissipation due to interaction with toroidally coupled Alfvén resonances.^{11,12} Hence, plasma dis-

sipation is associated with internal Alfvén resonances in the latest RWM theories.^{13,14} Fitzpatrick and Aydemir have developed a simplified cylindrical model of this rather complicated stabilization mechanism in which the required plasma dissipation is provided by edge plasma viscosity.¹⁵ In the latter model, the dispersion relation of the RWM reduces to a simple *cubic* equation. Nevertheless, the predictions of the Fitzpatrick–Aydemir model agree surprisingly well with the more sophisticated models of Bondeson, Betti, and co-workers. According to all models, the critical toroidal plasma velocity required to stabilize the RWM is of order $(k_{\parallel}a)V_a$, where k_{\parallel} is the parallel (to the magnetic field) wave number of the mode at the edge of the plasma, a the plasma minor radius, and V_a the typical Alfvén velocity. It turns out that external-kink modes are only unstable in tokamak plasmas when $k_{\parallel}a \ll 1$. Hence, the critical rotation velocity is only a few percent (5%, say) of the Alfvén velocity. Such velocities are regularly generated when present-day tokamaks are heated via unbalanced neutral beam injection (NBI). Although plasma dissipation is needed for the stabilization of the RWM, the width of the stability window (in β) becomes independent of the dissipation once it exceeds a (small) critical magnitude. This fact helps to explain why the Fitzpatrick–Aydemir model agrees fairly well with the models of Bondeson, Betti, and co-workers, despite the somewhat different dissipation mechanism in the former model.

The physics of the RWM has been investigated extensively on the DIII-D tokamak.^{16,17} The critical plasma toroidal angular frequency at the $q=2$ surface required to stabilize the mode is observed to be $\Omega_c/2\pi \sim 6$ kHz. The models of Bondeson, Betti, and co-workers, which depend on plasma dissipation at internal Alfvén resonances, predict $\Omega_c/2\pi \sim 10$ kHz. Other theories which require the formation of internally resonant magnetic islands,¹⁸ or linear tearing layers,¹⁹ for RWM stabilization yield much smaller critical frequencies: $\Omega_c/2\pi \sim 50$ Hz. The models of Bondeson, Betti, and co-workers agree fairly well with experiment. On the other hand, the predictions of the remaining models disagree with experimental observations to such an extent that they can be safely ruled out.

The plasma rotation in DIII-D starts to *decelerate* as

^{a)}Electronic mail: rfitzp@farside.ph.utexas.edu

soon as the no-wall β limit is exceeded. The deceleration occurs in three distinct phases: a slowly decreasing plasma rotation with little or no mode activity, followed by a more rapid deceleration of the rotation as a slowly growing mode appears, followed by a rapid growth of the mode. The latter phase is usually terminated by a plasma disruption. To date, the only theory to investigate the effect of the RWM on plasma rotation is that of Gimblett and Hastie.²⁰ The Gimblett–Hastie model yields predictions which are in qualitative agreement with DIII-D experimental data. However, this model relies on dissipation via an internally resonant linear tearing layer—as has already been discussed, such a dissipation mechanism gives far too low a critical plasma rotation frequency needed to stabilize the RWM.

The deceleration of DIII-D plasmas after the no-wall β limit is exceeded seems to be related to the magnitude of the resonant *error field*. It is certainly the case that a plasma can be maintained above the no-wall β limit for the longest period when the error field is minimized. Conversely, plasmas with large error fields tend to disrupt prematurely when the β limit is exceeded. There is experimental evidence that the error field is strongly *amplified* by the plasma when β lies above the no-wall limit. Hence, it is conjectured that the plasma deceleration observed in DIII-D is associated with the nonlinear locking torque generated by an amplified error field. Recently, Boozer has developed a general theory which implies that error-field amplification peaks strongly as the no-wall β limit is achieved.²¹ However, this theory is too empirical to allow quantitative predictions.

The aim of this paper is to construct a simple *physics-based* model of the RWM which accounts for the DIII-D data. This goal will be achieved by combining the Fitzpatrick–Aydemir dispersion relation with a plasma equation of rotational motion.

II. THE FITZPATRICK–AYDEMIR DISPERSION RELATION

A. Definitions

Consider the stability of the m, n mode—which is assumed to be *non-resonant*—in a cylindrical, zero- β plasma. Standard right-handed polar coordinates (r, θ, z) are adopted. The plasma is assumed to be periodic in the z direction with period $2\pi R_0$, where R_0 is the simulated major radius. It is convenient to define the simulated toroidal angle $\phi = z/R_0$. The equilibrium magnetic field is written $[0, B_\theta(r), B_\phi]$. Finally, the “safety factor” is defined $q(r) = rB_\phi/R_0B_\theta$.

Let a be the minor radius of the plasma, r_w the minor radius of the resistive wall, and r_c the critical wall radius (i.e., the minor radius beyond which a perfectly conducting wall is incapable of stabilizing the m, n ideal external-kink mode). It is helpful to define

$$d = \frac{1}{m} \frac{(r_w/a)^{2m} - 1}{(r_w/a)^{2m} + 1}, \quad (1)$$

$$d_c = \frac{1}{m} \frac{(r_c/a)^{2m} - 1}{(r_c/a)^{2m} + 1}, \quad (2)$$

$$c = \frac{m/n - q(a)}{s(a)q(a)}, \quad (3)$$

where $s(r) = (r/q)(dq/dr)$ is the magnetic shear.

The radial magnetic field associated with the m, n mode can be written

$$b_r^{m,n}(r, \theta, \phi, t) = i \frac{m}{r} \psi(r) e^{i(m\theta - n\phi) + \gamma t}. \quad (4)$$

B. Plasma physics

The Fitzpatrick–Aydemir model assumes that the m, n rational surface, on which $q = m/n$, lies *just beyond* the edge of the plasma. Hence, $0 < c \ll 1$. The bulk of the plasma is governed by conventional, marginally stable, ideal magneto-hydrodynamics (MHD). However, a thin *inertial* layer, of thickness ca , forms at the outer edge of the plasma. An even thinner *viscous* layer forms at the outer edge of the inertial layer. The response of the plasma is fully described by the quantity $\Delta \Psi_a = [r d\psi/dr]_{a-}^{a+}$. According to Ref. 15, this quantity takes the approximate form

$$d\Delta \Psi_a \approx [(\hat{\gamma} - i\hat{\Omega}_\phi)^2 + \nu_* (\hat{\gamma} - i\hat{\Omega}_\phi)] \Psi_a, \quad (5)$$

where $\Psi_a = \psi(a)$, $\hat{\gamma} = \gamma/n\Omega_0$, $\hat{\Omega}_\phi = \Omega_\phi/\Omega_0$,

$$\Omega_0 \tau_A = \sqrt{\frac{3c}{d}} \frac{cs(a)}{1 - c/d_c}, \quad (6)$$

$$\nu_* = \frac{12}{5c^2 \tau_V n \Omega_0}, \quad (7)$$

and $\tau_A = (R_0/B_\phi) \sqrt{\mu_0 \rho(a)}$, $\tau_V = a^2 \rho(a)/\mu(a)$. Here, Ω_ϕ is the plasma toroidal angular velocity within the inertial layer, $\rho(r)$ the plasma mass density, and $\mu(r)$ the perpendicular viscosity. In Eq. (5), the first term inside the square brackets corresponds to plasma *inertia*, whereas the second term corresponds to *viscous dissipation*. The parameter ν_* measures the strength of this dissipation. Note that Eq. (5) is derived under the assumption that the plasma dissipation is relatively weak (i.e., $\nu_* \ll 1$).

C. Wall physics

The L/R time of the resistive wall is defined $\tau_w = \mu_0 r_w \delta_w / \eta_w$, where δ_w and η_w are the wall thickness and resistivity, respectively. The response of the wall is fully described by the quantity $\Delta \Psi_w = [r d\psi/dr]_{r_w-}^{r_w+}$. In the “thin shell” limit, in which $\delta_w/r_w \ll |\gamma| \tau_w \ll r_w/\delta_w$, this quantity takes the form

$$d\Delta \Psi_w = \hat{\gamma} S_* \Psi_w, \quad (8)$$

where $\Psi_a = \psi(r_w)$ and $S_* = d\tau_w n \Omega_0$. The parameter S_* (which is assumed to be much larger than unity) measures the conductivity of the wall.

D. Outer solution

The quantities $\Delta\Psi_a$ and $\Delta\Psi_w$ must be asymptotically matched to the outer solution, which is governed by marginally stable ideal MHD. As described in Ref. 15, this matching procedure yields

$$d\Delta\Psi_a = -(1-\kappa)(1-md)\Psi_a + \sqrt{1-(md)^2}\Psi_w, \quad (9)$$

$$d\Delta\Psi_w = -(1+md)\Psi_w + \sqrt{1-(md)^2}\Psi_a + 2md\Psi_c. \quad (10)$$

Here,

$$\kappa = \frac{(1/d_c) - m}{(1/d) - m} \quad (11)$$

measures the intrinsic stability of the plasma in the absence of rotation. The no-wall stability limit (i.e., the stability limit in the complete absence of a wall) corresponds to $\kappa=0$, whereas the perfect-wall limit (i.e., the stability limit when the wall becomes perfectly conducting) corresponds to $\kappa=1$. Note, incidentally, that in the Fitzpatrick–Aydemir model the m, n mode is destabilized by *current gradients* rather than *pressure gradients*. The quantity Ψ_c parametrizes the m, n static error field— Ψ_c is actually defined as the error-field flux at the wall in the absence of plasma.

E. RWM dispersion relation

Neglecting the error field, for the moment, Eqs. (5), (8), (9), and (10) can be combined to give the following simple cubic RWM dispersion relation:

$$\begin{aligned} & [(\hat{\gamma} - i\hat{\Omega}_\phi)^2 + \nu_* (\hat{\gamma} - i\hat{\Omega}_\phi) + (1-\kappa)(1-md)] \\ & \times (\hat{\gamma} S_* + 1 + md) = 1 - (md)^2. \end{aligned} \quad (12)$$

F. Error-field amplification

Suppose that the plasma is stable, and subject to a *static* error field (hence, $\hat{\gamma}=0$, and $|\Psi_c| \neq 0$). Equations (5), (8), (9), and (10) can be combined to give

$$\frac{|\Psi_a|}{|\Psi_c|} = \left(\frac{1-md}{1+md} \right)^{1/2} \frac{2md}{\{[\hat{\Omega}_\phi^2 + \kappa(1-md)]^2 + (\nu_* \hat{\Omega}_\phi)^2\}^{1/2}}. \quad (13)$$

Clearly, the plasma response to the error field is *resonant* when $\kappa = \kappa_1$, where

$$\kappa_1 = - \frac{\hat{\Omega}_\phi^2}{1-md}. \quad (14)$$

The magnitude of the flux, $|\Psi_a|$, driven at the plasma edge peaks at the resonance—the strength of this peaking varies inversely with the size of the dissipation parameter, ν_* . This result is similar to that recently reported by Boozer.²¹

G. Low dissipation stability boundaries

In the low dissipation limit, $\nu_* \ll 1$, there are only two possibly unstable roots of the RWM dispersion relation (12). The *wall mode* root satisfies

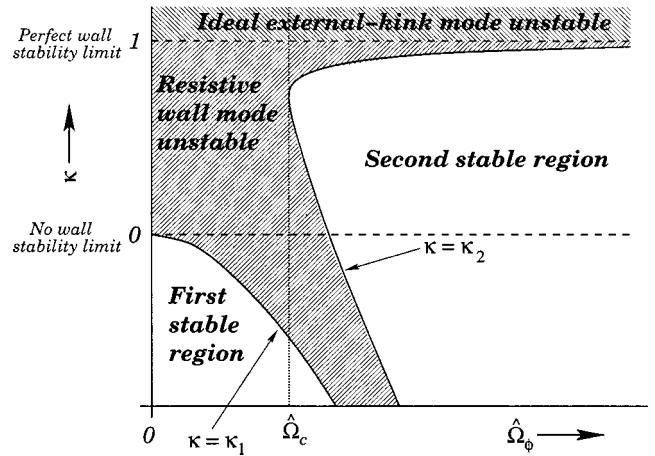


FIG. 1. Low dissipation stability boundaries for the resistive wall and ideal external-kink modes in plasma rotation ($\hat{\Omega}_\phi$) versus plasma stability (κ) space. The plasma becomes more unstable as κ increases.

$$\begin{aligned} \hat{\gamma} \approx & \frac{i[1-(md)^2]\nu_* \hat{\Omega}_\phi}{S_* [(1-\kappa)(1-md) - \hat{\Omega}_\phi^2]^2} \\ & + \frac{(1+md)[\kappa(1-md) + \hat{\Omega}_\phi^2]}{S_* [(1-\kappa)(1-md) - \hat{\Omega}_\phi^2]}, \end{aligned} \quad (15)$$

whereas the *plasma mode* root obeys

$$\begin{aligned} \hat{\gamma} \approx & i[\hat{\Omega}_\phi - \sqrt{(1-\kappa)(1-md)}] \\ & + \frac{1-(md)^2}{2S_* \sqrt{(1-\kappa)(1-md)}[\hat{\Omega}_\phi - \sqrt{(1-\kappa)(1-md)}]} \\ & - \frac{\nu_*}{2}. \end{aligned} \quad (16)$$

The marginal stability condition for the wall mode root coincides with the error-field resonance: i.e., $\kappa = \kappa_1$. The marginal stability condition for the plasma mode root takes the form $\kappa = \kappa_2$, where κ_2 is obtain by solving the quadratic equation $x^2 - \hat{\Omega}_\phi x + \epsilon = 0$, with $x = \sqrt{(1-\kappa_2)(1-md)}$ and $\epsilon = [1-(md)^2]/S_* \nu_*$. Figure 1 shows a sketch of the low dissipation stability boundaries for the resistive wall and ideal external-kink modes in $\kappa - \hat{\Omega}_\phi$ space. It can be seen that there are two separate stable regions. The first stable region is restricted to low κ and $\hat{\Omega}_\phi$ values, and is bounded by the curve $\kappa = \kappa_1$. The second stable region only exists for finite $\hat{\Omega}_\phi$, and is bounded by the curve $\kappa = \kappa_2$. In fact, the critical (normalized) plasma rotation rate above which this region appears is

$$\hat{\Omega}_c = \frac{2\sqrt{1-(md)^2}}{\sqrt{S_* \nu_*}}. \quad (17)$$

Hence, it can be seen that there is no second stable region in the absence of plasma dissipation (i.e., $\nu_* \rightarrow 0$). Note that the boundaries of the second stable region rapidly become inde-

pendent of ν_* as $\hat{\Omega}_\phi$ increases. Note, also, that the upper boundary of this region lies very close to the perfect-wall stability limit, $\kappa = 1$.

It is evident, from Fig. 1, that the stability boundary for the first stable region, $\kappa = \kappa_1$, decreases as the plasma rotation increases. In other words, plasma rotation initially has a destabilizing effect on the RWM.^{9,10,15} Somewhat higher levels of rotation cause a transition to the second stable region. Thus, high levels of rotation have a stabilizing effect on the RWM.^{9,10,15} Note that there is a finite-width band of instability separating the first and second stable regions.¹⁰

H. High dissipation stability boundaries

In the high dissipation limit, $\nu_* \gg 1$, there are again two possibly unstable roots of the RWM dispersion relation (12). The wall mode root satisfies

$$\hat{\gamma} \approx \frac{1 + md}{S_*} \left\{ \frac{\kappa(1 - \kappa)(1 - md)^2 - \nu_*^2 \hat{\Omega}_\phi^2}{(1 - \kappa)^2(1 - md)^2 + \nu_*^2 \hat{\Omega}_\phi^2} + \frac{i \nu_* \hat{\Omega}_\phi}{(1 - \kappa)^2(1 - md)^2 + \nu_*^2 \hat{\Omega}_\phi^2} \right\}, \tag{18}$$

whereas the plasma mode root obeys

$$\hat{\gamma} \approx \frac{(\kappa - 1)(1 - md)}{\nu_*} + i\Omega. \tag{19}$$

In this limit, the dissipative layer at the edge of the plasma becomes wider than the inertial layer, and plasma inertia ceases to play a significant role in RWM physics. Incidentally, the above roots are identical to those obtained from the well-known dispersion relation of Bondeson and Persson²² for an edge tearing mode coupled to a resistive wall. This observation gives us confidence that the dispersion relation (12) remains valid when $\nu_* \gg O(1)$, despite the fact that it was derived in the limit $\nu_* \ll 1$.

The marginal stability condition for the wall mode root is written $\kappa = \kappa_3$, where $\kappa_3(1 - \kappa_3) = \alpha$. Here, $\alpha = \nu_*^2 \hat{\Omega}_\phi^2 / (1 - md)^2$. The marginal stability condition for the plasma mode root is simply $\kappa = 1$. The RWM is completely stabilized (for $\kappa < 1$) as soon as the (normalized) plasma rotation exceeds the critical value $\hat{\Omega}_c$, where

$$\hat{\Omega}_c = \frac{1 - md}{2\nu_*}. \tag{20}$$

Figure 2 shows a sketch of the high dissipation stability boundaries for the resistive wall and ideal external-kink modes in $\kappa - \hat{\Omega}_\phi$ space. It can be seen that, in the high dissipation regime, the first and second stable regions of Fig. 1 merge together to form a continuous stable region which extends all the way to the perfect-wall stability boundary.

I. Intermediate dissipation stability boundaries

Figure 3 shows the numerically determined stability boundaries of the Fitzpatrick–Aydemir dispersion relation calculated for various values of the dissipation parameter,

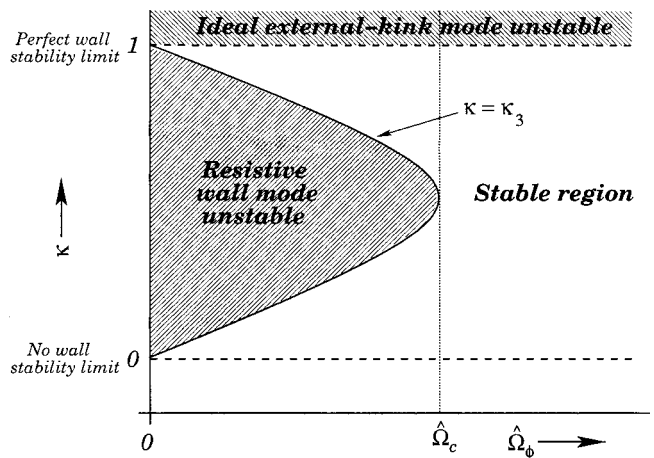


FIG. 2. High dissipation stability boundaries for the resistive wall and ideal external-kink modes in plasma rotation ($\hat{\Omega}_\phi$) versus plasma stability (κ) space. The plasma becomes more unstable as κ increases.

ν_* . When the dissipation is low (i.e., $\nu_* = 0.1$), there is a band of instability separating the first and second stable regions (as sketched in Fig. 1). However, this band gradually closes up as the dissipation increases. Thus, when ν_* reaches 0.5 there is only a vestigial band, and when ν_* reaches 1.0 the band has disappeared entirely (as sketched in Fig. 2).

Note that the error-field resonance, $\kappa = \kappa_1$, corresponds, almost exactly, to the lower stability boundary for $\nu_* = 0.1$ shown in Fig. 3. It is clear from the figure that, unless the dissipation is fairly weak (i.e., $\nu_* \leq 0.1$), the error-field resonance does not correspond to a RWM stability boundary. The reason for this is that, unless ν_* is small, the RWM possesses a non-negligible real frequency at its marginal stability point. It is easily demonstrated that a real frequency of order the inverse wall time is sufficient to shift the error-field resonance (which corresponds to the response of the plasma to a zero frequency perturbation) away from the RWM stability boundary.

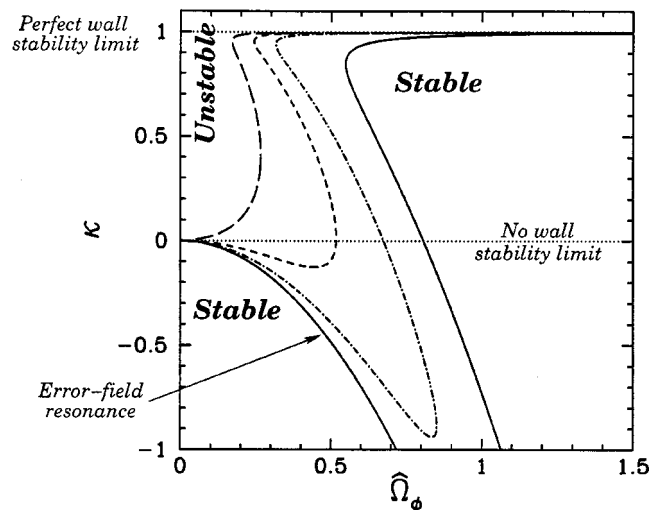


FIG. 3. Stability boundaries for the Fitzpatrick–Aydemir RWM dispersion relation, evaluated numerically for $\nu_* = 0.10$ (solid curve), $\nu_* = 0.30$ (dotted–dashed curve), $\nu_* = 0.50$ (short-dashed curve), and $\nu_* = 1.00$ (long-dashed curve), as well as $S_* = 100$, $m = 3$, and $r_w = 1.2a$.

III. DERIVATION OF EVOLUTION EQUATIONS

A. Plasma angular equation of motion

The toroidal angular equation of motion of the inertial layer (radial thickness ca) at the edge of the plasma takes the approximate form

$$a^2 c \rho(a) \frac{d\Omega_\phi}{dt} + \frac{12}{5} \frac{\mu(a)}{c} (\Omega_\phi - \Omega_\phi^{(0)}) = \frac{T_{\phi \text{ EM}}}{4\pi^2 R_0^3}, \quad (21)$$

where $\Omega_\phi^{(0)}$ is the unperturbed rotation rate, and $T_{\phi \text{ EM}}$ is the electromagnetic torque acting on the layer due to the error-field and eddy currents excited in the resistive wall. The first term on the left-hand side of the above equation corresponds to the inertia of the layer, whereas the second term describes the viscous restoring torque exerted by the remainder of the plasma.

The electromagnetic torque takes the form²³

$$T_{\phi \text{ EM}} = \frac{2\pi^2 R_0}{\mu_0} n \text{Im}(\Delta \Psi_a \Psi_a^*), \quad (22)$$

B. Normalized evolution equations

Let

$$\hat{\Psi}_{a,w,c} = \frac{\Psi_{a,w,c}}{aB_\phi \sqrt{2cd\tau_A} \Omega_0}, \quad (23)$$

and $\hat{\Omega}_\phi^{(0)} = \Omega_\phi^{(0)}/\Omega_0$. Equations (5), (8), (9), (10), and (21) can be combined to give

$$\begin{aligned} \frac{d^2 \hat{\Psi}_a}{d\hat{t}^2} + (\nu_* - 2i\hat{\Omega}_\phi) \frac{d\hat{\Psi}_a}{d\hat{t}} \\ + [(1-\kappa)(1-md) - \hat{\Omega}_\phi^2 - i\nu_* \hat{\Omega}_\phi] \hat{\Psi}_a \\ = \sqrt{1-(md)^2} \hat{\Psi}_w, \end{aligned} \quad (24)$$

$$\begin{aligned} S_* \frac{d\hat{\Psi}_w}{d\hat{t}} + (1+md) \hat{\Psi}_w \\ = \sqrt{1-(md)^2} \hat{\Psi}_a + 2md \hat{\Psi}_c, \end{aligned} \quad (25)$$

$$\begin{aligned} \frac{d\hat{\Omega}_\phi}{d\hat{t}} + \nu_* (\hat{\Omega}_\phi - \hat{\Omega}_\phi^{(0)}) \\ = \sqrt{1-(md)^2} \text{Im}(\hat{\Psi}_w \hat{\Psi}_a^*), \end{aligned} \quad (26)$$

where $\hat{t} = n\Omega_0 t$. Here, Eqs. (5), (8), (9), and (10) have been conveniently converted into ordinary differential equations. The basic approach adopted in this paper is to treat the S_* , ν_* , and the normalizations as constant, while allowing κ , $\hat{\Omega}_\phi^{(0)}$, and $\hat{\Psi}_c$ to vary. This is not quite self-consistent. However, the dependencies of S_* , ν_* , and the normalizations on κ are physically unimportant. Note that it makes sense to combine the *linear* Fitzpatrick–Aydemir dispersion relation for the RWM with a *non-linear* plasma equation of rotational motion because the critical RWM amplitude above which the

plasma rotation is effectively quenched is very small compared with the equilibrium magnetic field strength (see Sec. IV).

It is helpful to express the electromagnetic torque on the right-hand side of Eq. (26) in a more physically meaningful form. Writing $\hat{\Psi}_w = |\hat{\Psi}_w| e^{i\varphi_w}$, Eq. (25) yields

$$\begin{aligned} \sqrt{1-(md)^2} \text{Im}(\hat{\Psi}_w \hat{\Psi}_a^*) = -S_* \frac{d\varphi_w}{d\hat{t}} |\hat{\Psi}_w|^2 \\ - 2md \text{Im}(\hat{\Psi}_w \hat{\Psi}_c^*). \end{aligned} \quad (27)$$

Thus, the torque consists of the familiar slowing down torque due to eddy currents excited in the wall, plus a conventional error-field locking torque.²⁴ Now, $|\hat{\Psi}_w|$ and φ_w can only evolve on the relatively slow L/R time of the wall. Setting $d/d\hat{t} \sim 1/S_*$ in Eqs. (24) and (25), and recalling that $S_* \gg 1$, it is possible to show that

$$\begin{aligned} -S_* \frac{d\varphi_w}{d\hat{t}} |\hat{\Psi}_w|^2 - 2md \text{Im}(\hat{\Psi}_w \hat{\Psi}_c^*) \approx -\nu_* \hat{\Omega}_\phi |\hat{\Psi}_a|^2. \end{aligned} \quad (28)$$

It follows that the electromagnetic torque always acts to *damp* the plasma rotation. Moreover, there is zero torque in the absence of plasma dissipation (i.e., $\nu_* = 0$).

Equations (24)–(26) can be rewritten

$$\begin{aligned} \frac{d^2 \hat{\Psi}_a}{d\hat{t}^2} + (\nu_* - 2i\hat{\Omega}_\phi) \frac{d\hat{\Psi}_a}{d\hat{t}} \\ + [(1-\kappa)(1-md) - \hat{\Omega}_\phi^2 - i\nu_* \hat{\Omega}_\phi] \hat{\Psi}_a \\ = \sqrt{1-(md)^2} \hat{\Psi}_w, \end{aligned} \quad (29)$$

$$S_* \frac{d\hat{\Psi}_w}{d\hat{t}} + (1+md) \hat{\Psi}_w = \sqrt{1-(md)^2} \hat{\Psi}_a + 2md \hat{\Psi}_c, \quad (30)$$

$$\frac{d\hat{\Omega}_\phi}{d\hat{t}} + \nu_* (\hat{\Omega}_\phi - \hat{\Omega}_\phi^{(0)}) = -\nu_* \hat{\Omega}_\phi |\hat{\Psi}_a|^2. \quad (31)$$

These equations constitute a closed set which describe the evolution of the RWM in the presence of a static error field, taking into account the nonlinear effect of the mode on the plasma rotation. The dynamic variables are the plasma flux, $\hat{\Psi}_a$, the wall flux, $\hat{\Psi}_w$, and the plasma rotation, $\hat{\Omega}_\phi$. The parameters ν_* , S_* , κ , $\hat{\Omega}_\phi^{(0)}$, and $\hat{\Psi}_c$ specify the strength of the plasma dissipation, the conductivity of the wall, the stability of the plasma, the unperturbed plasma rotation, and the amplitude and phase of the error field, respectively. The additional parameters m and d specify the poloidal mode number of the RWM, and the radius of the wall, respectively.

IV. NUMERICAL SIMULATIONS

A. Introduction

This section describes a number of simulations performed by integrating the RWM evolution equations, (29)–(31).

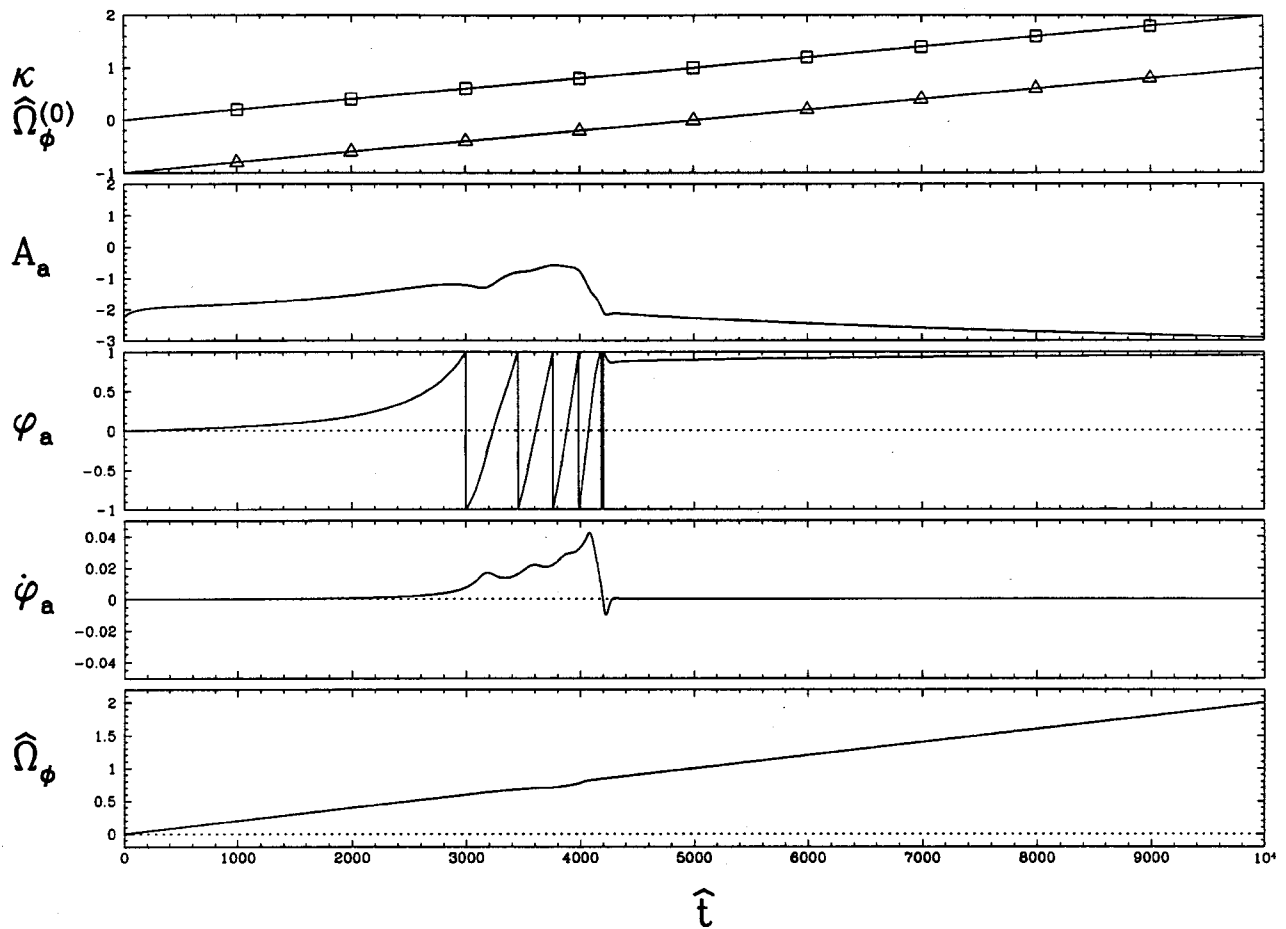


FIG. 4. Simulation of a DIII-D NBI heating ramp in which the equilibrium plasma rotation and stability parameters increase linearly. The other parameters are $\Psi_c = 0.01$, $\nu_* = 0.33$, $S_* = 100$, $m = 3$, and $r_w = 1.2a$. The five panels show (1) the stability parameter, κ (triangles), and the equilibrium rotation parameter, $\hat{\Omega}_\phi^{(0)}$ (squares), (2) the mode amplitude parameter, $A_a = \log_{10}(|\Psi_a|)$, (3) the mode phase, $\varphi_a = \arg(\Psi_a)$ (units of π), (4) the mode phase velocity, $\dot{\varphi}_a = d\varphi/d\hat{t}$, (5) the plasma rotation parameter, $\hat{\Omega}_\phi$.

B. Access to the wall stabilized region: $\nu_* = 0.33$

According to Sec. II, when the dissipation parameter ν_* is less than about 0.5 there are two separate stable regions in $\hat{\Omega}_\phi - \kappa$ space (see Fig. 1). The first region is restricted to relatively low $\hat{\Omega}_\phi$ values, and lies well below the perfect-wall stability boundary ($\kappa = 1$). The second region only exists for $\hat{\Omega}_\phi > \hat{\Omega}_c$, where $\hat{\Omega}_c$ [see Eq. (17)] is the critical rotation rate needed to stabilize the RWM, and extends nearly all the way to the perfect-wall stability boundary. Clearly, in order to obtain strongly enhanced plasma stability, due to the presence of the resistive wall, it is necessary for the plasma to make a transition from the first stable region (in which it starts off) to the second stable region. This transition is initiated when the NBI power is ramped up, and the plasma rotation and β (or, in this paper, κ) consequently increase. Unfortunately, in order to reach the second stable region, the plasma must first pass through a region of parameter space in which the RWM is *unstable*. Let us simulate the transition process, using realistic plasma parameters and NBI heating rates, in order to determine which factors effectively control access to the second stable region.

The chosen plasma parameters for our study are $\nu_* = 0.33$, $S_* = 100$, $m = 3$, and $r_w = 1.2a$. These values are ap-

propriate to the RWM in DIII-D (see Sec. IV D). The error-field parameter, $\hat{\Psi}_c$, is taken to be *real*. Hence, the helical phase of the error field is 0° . Figure 4 shows details of a simulation in which $\hat{\Psi}_c = 0.01$, and the plasma equilibrium rotation and stability parameters, $\hat{\Omega}_\phi^{(0)}$ and κ , are ramped linearly over a period of 10^4 normalized time units (i.e., about 100 wall L/R times). Figure 5 shows the trajectory of the same simulation through $\hat{\Omega}_\phi - \kappa$ space.

Note, first of all, from Fig. 5, that the first and second stable regions *merge* below $\kappa \approx -0.7$ (see Sec. III). In the initial stage of the ramp (i.e., $\hat{t} < 2500$), the plasma traverses the first stable region. During this phase, the m, n mode is maintained in the plasma by the error field. Note that the mode is initially locked in phase with the error field. However, as the boundary of the first stable region is approached, the mode becomes increasingly phase shifted (in the direction of plasma rotation) with respect to the error field, and the mode amplitude increases. This increase in the mode amplitude is a manifestation of enhanced error-field amplification at the error-field resonance (see Sec. II F), which lies fairly close to the boundary of the first stable region. In the middle stage of the ramp (i.e., from $\hat{t} \approx 2500$ to $\hat{t} \approx 4500$), the

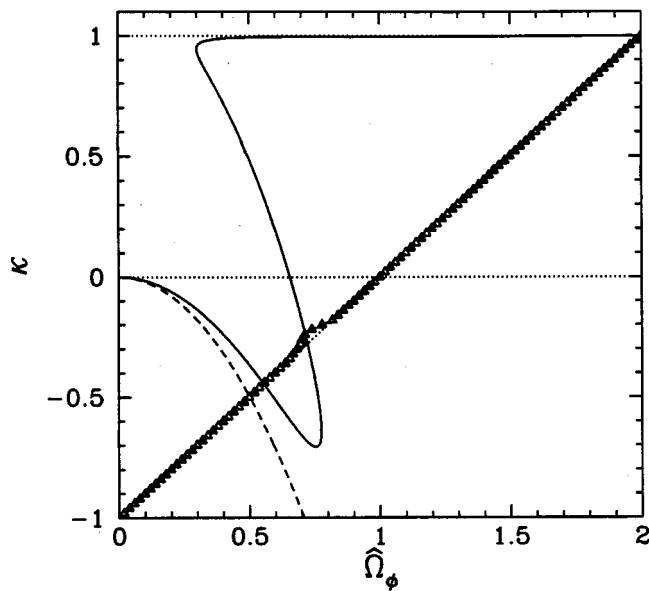


FIG. 5. The trajectory (triangles) of the simulation shown in Fig. 4 plotted at equal time intervals in $\hat{\Omega}_\phi - \kappa$ space. The dashed curve shows the error-field resonance. The solid curve shows the stability boundary for the RWM.

plasma traverses the band of instability separating the first and second stable regions. During this phase, the mode *unlocks* from the error field and *grows* spontaneously. The mode rotates at about the inverse wall L/R time (i.e., $d\phi_a/d\hat{t} \sim S_*^{-1}$). Note that the mode amplitude never becomes sufficiently large to trigger plasma deceleration. Hence, the plasma rotation, $\hat{\Omega}_\phi$, always tracks the equilibrium rotation, $\hat{\Omega}_\phi^{(0)}$, very closely. In the final stage of the ramp (i.e., $\hat{t} > 4500$), the plasma traverses the second stable region. During this phase, the mode is again maintained in the plasma by the error field. The mode amplitude drops rapidly as the plasma enters the second stable region, and eventually reaches an equilibrium value which is significantly less than the typical value in the first stable region. Clearly, error-field amplification is a far smaller effect in the second stable region when compared with the first, since the latter region lies closer to the error-field resonance. Note that the mode locks in *antiphase* with the error field in the second stable region (however, the wall flux, $\hat{\Psi}_w$ still locks *in phase* with the error field).

Figures 6 and 7 show the results of a second simulation whose parameters are the same as the first, except that the amplitude of the error field is increased to $\hat{\Psi}_c = 0.02$. It can be seen that the mode evolution remains similar to that shown in the first simulation up to the period when the plasma traverses the band of instability separating the two stable regions. During this period, the mode grows to sufficient amplitude to trigger plasma deceleration. This is indicated in Fig. 7 by the sudden deviation of the simulation trajectory upwards and to the left. From Fig. 6, it can be seen that the plasma rotation ceases its linear increase, and actually starts to *decrease*, despite the fact that more and more “momentum” is being injected into the plasma (i.e., $\hat{\Omega}_\phi^{(0)}$ is

increasing). The deceleration of the plasma effectively prevents access to the second stable region and takes place in three main stages. In the first stage, the mode amplitude is slowly increasing, and there is no plasma deceleration. In the second stage, the mode amplitude increases somewhat faster, and the plasma rotation slowly ramps down. During this phase, the rate of deceleration is limited by the fact that the plasma cannot re-enter the first stable region—if it did, the mode would decay, and the plasma would consequently re-rotate. Hence, as can be seen from Fig. 7, the simulation trajectory remains just outside the boundary of the first stable region. In the final stage, the continued κ ramp takes the plasma away from the boundary of the first stable region. During this phase, the plasma rotation collapses completely, and the mode grows rapidly—indeed, the mode amplitude quickly attains values which would (presumably) trigger a disruption. The behavior described above is quite similar to that seen in the DIII-D experiment.

The above simulations suggest that there are three main factors which govern access to the wall stabilized region: the magnitude of the *error field*, the rate at which the plasma *rotation* is ramped, and the strength of the plasma *dissipation*.

The magnitude of the error field determines the mode amplitude as the plasma enters the band of instability separating the two stable regions. If this amplitude is too high (i.e., if the error field is too large) then the mode is able to grow sufficiently large to trigger plasma deceleration before the plasma reaches the other side of the band—hence, the plasma is prevented from accessing the second stable region.

The faster the rotation is ramped, the less time the plasma spends traversing the unstable band, and hence, the less time the mode has in which to grow to a dangerous amplitude. It follows that a fast NBI ramp rate facilitates entry into the second stable region.

As can be seen from Fig. 3, the width of the unstable band separating the first and second stable regions is a rapidly decreasing function of increasing plasma dissipation, ν_* . Hence, increased dissipation is likely to favor entry into the second stable region.

C. Access to the wall stabilized region: $\nu_* = 0.66$

According to Sec. II, when the dissipation parameter ν_* exceeds about 0.5 the first and second stable regions merge to form a region of stability which extends all the way to the perfect-wall stability boundary ($\kappa = 1$). Under these circumstances, it is possible for an NBI-induced ramp in κ and $\hat{\Omega}_\phi$ to take the plasma to the perfect-wall stability boundary without the RWM ever becoming unstable. This is illustrated in Figs. 8 and 9, which show details of a simulation in which $\nu_* = 0.66$, $S_* = 100$, $m = 3$, $r_w = 1.2a$, $\hat{\Psi}_c = 0.05$, and the equilibrium rotation and stability parameters, $\hat{\Omega}_\phi$ and κ , are ramped linearly over a period of about 100 wall L/R times. These parameter values are appropriate to the RWM in DIII-D (see Sec. IV D).

It can be seen, from Fig. 9, that the plasma remains stable throughout the duration of the simulated NBI ramp.

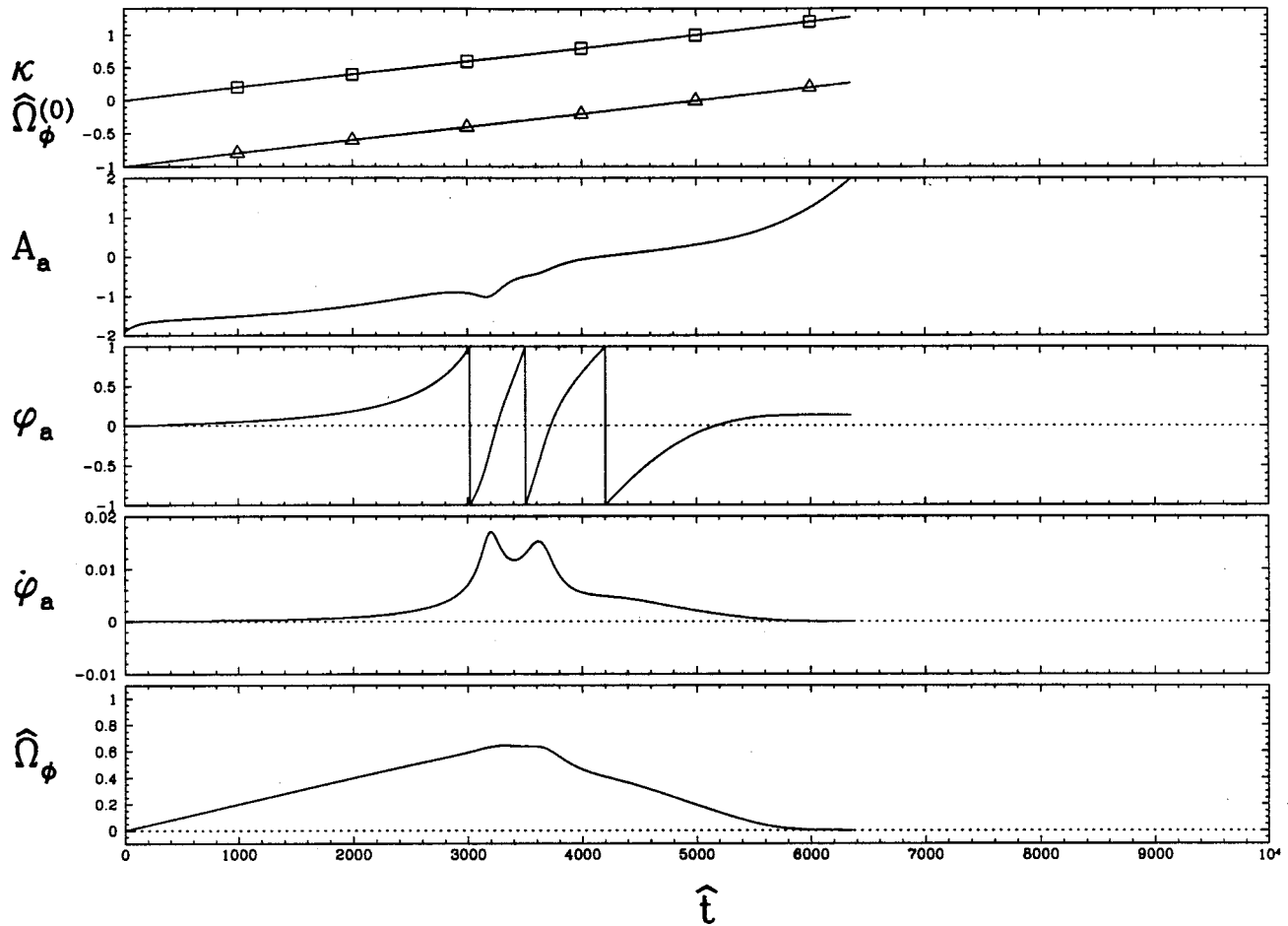


FIG. 6. Simulation of a DIII-D NBI heating ramp in which the equilibrium plasma rotation and stability parameters increase linearly. The other parameters are $\Psi_c = 0.02$, $\nu_* = 0.33$, $S_* = 100$, $m = 3$, and $r_w = 1.2a$. The five panels show (1) the stability parameter, κ (triangles), and the equilibrium rotation parameter, $\Omega_\phi^{(0)}$ (squares), (2) the mode amplitude parameter, $A_a = \log_{10}(|\Psi_a|)$, (3) the mode phase, $\varphi_a = \arg(\Psi_a)$ (units of π), (4) the mode phase velocity, $\dot{\varphi}_a = d\varphi/d\hat{t}$, (5) the plasma rotation parameter, $\hat{\Omega}_\phi$.

Nevertheless, the plasma comes very close to the RWM stability boundary shortly after the no-wall stability boundary ($\kappa = 0$) is exceeded. According to Fig. 8, the mode amplitude peaks as the plasma crosses the error-field resonance, which happens somewhat before the no-wall stability boundary is reached. As the plasma grazes the RWM stability boundary there are induced oscillations in the mode amplitude and phase, but the mode does not unlock from the error field and its amplitude never becomes sufficiently large to trigger plasma deceleration.

Figures 10 and 11 show details of a second simulation whose parameters are the same as the previous simulation, except that the error-field amplitude has been increased to $\Psi_c = 0.1$. It can be seen that as the plasma crosses the error-field resonance the mode amplitude becomes sufficiently large to trigger plasma deceleration. This deceleration modifies the plasma trajectory in $\hat{\Omega}_\phi - \kappa$ space such that it intersects the RWM stability boundary. As soon as this occurs, the RWM becomes unstable and unlocks from the error field. After a few mode rotations, the plasma rotation collapses completely and the mode amplitude starts to grow, quickly

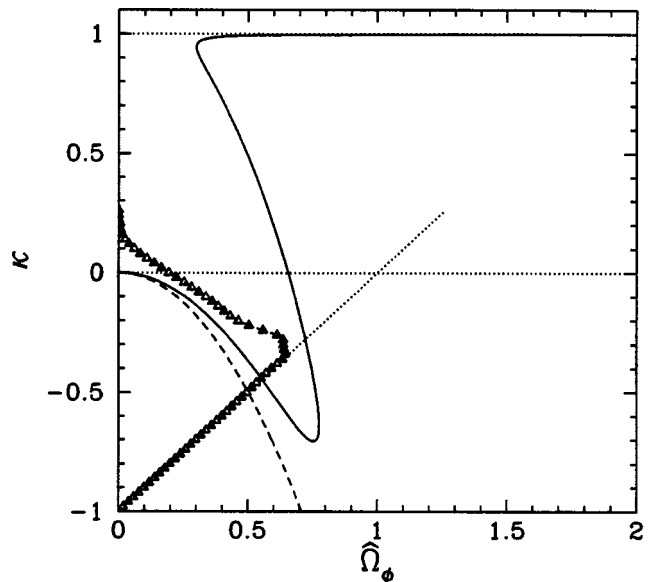


FIG. 7. The trajectory (triangles) of the simulation shown in Fig. 6 plotted at equal time intervals in $\hat{\Omega}_\phi - \kappa$ space. The dashed curve shows the error-field resonance. The solid curve shows the stability boundary for the RWM.

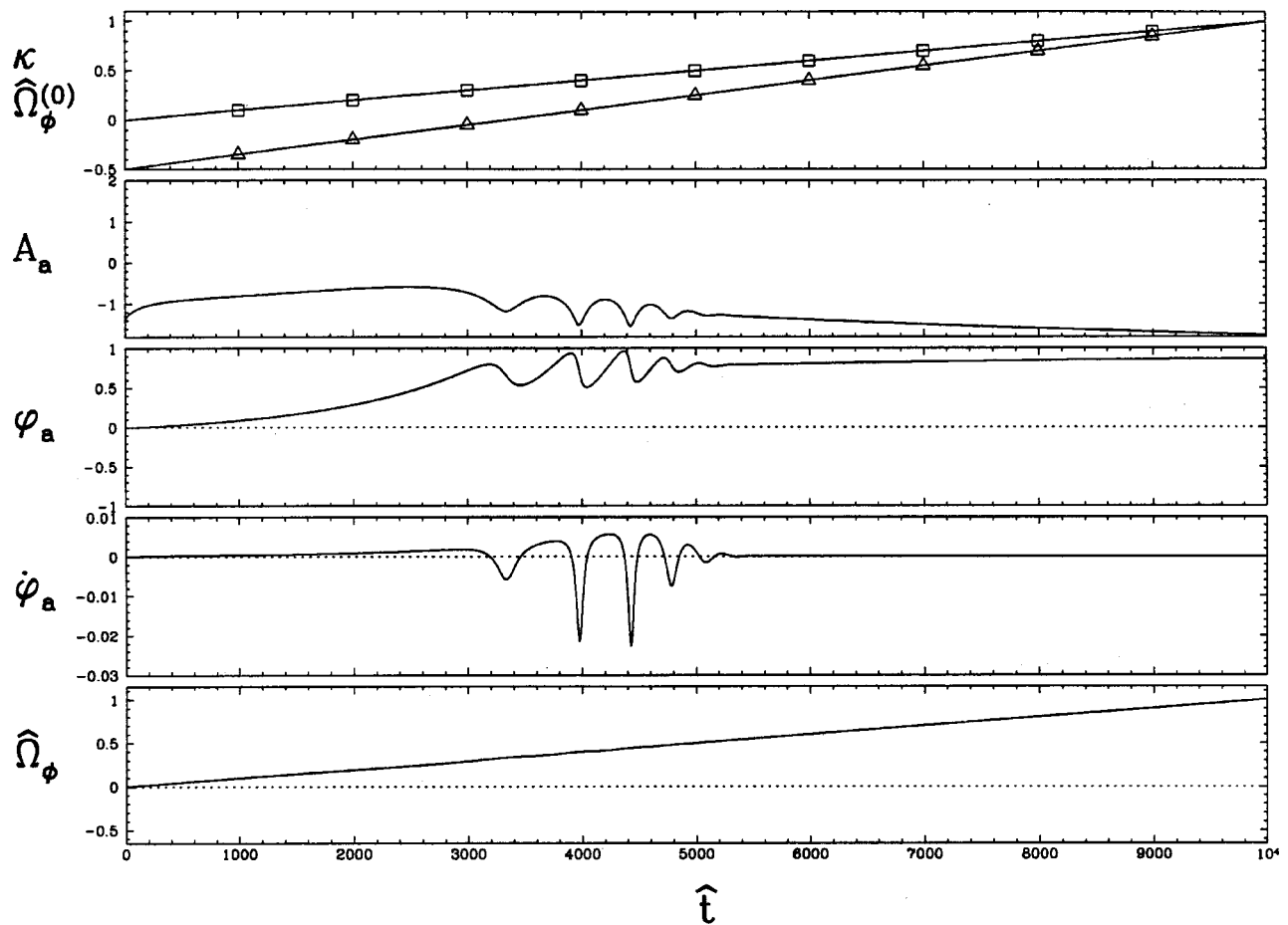


FIG. 8. Simulation of a DIII-D NBI heating ramp in which the equilibrium plasma rotation and stability parameters increase linearly. The other parameters are $\Psi_c = 0.05$, $\nu_* = 0.66$, $S_* = 100$, $m = 3$, and $r_w = 1.2a$. The five panels show (1) the stability parameter, κ (triangles), and the equilibrium rotation parameter, $\hat{\Omega}_\phi^{(0)}$ (squares), (2) the mode amplitude parameter, $A_a = \log_{10}(|\Psi_a|)$, (3) the mode phase, $\varphi_a = \arg(\Psi_a)$ (units of π), (4) the mode phase velocity, $\dot{\varphi}_a = d\varphi/d\hat{t}$, (5) the plasma rotation parameter, $\hat{\Omega}_\phi$.

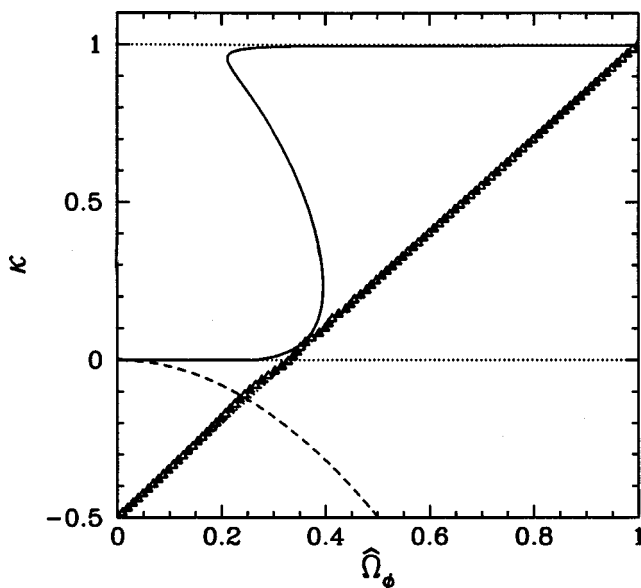


FIG. 9. The trajectory (triangles) of the simulation shown in Fig. 8 plotted at equal time intervals in $\hat{\Omega}_\phi - \kappa$ space. The dashed curve shows the error-field resonance. The solid curve shows the stability boundary for the RWM.

reaching values which would (presumably) trigger a disruption.

The above simulations confirm that the three main factors which govern access to the wall stabilized region are the magnitude of the *error field*, the rate at which the plasma *rotation* is ramped, and the strength of the plasma *dissipation*.

The magnitude of the error field determines the maximum mode amplitude: i.e., the amplitude as the plasma crosses the error-field resonance. If this amplitude is too high (i.e., if the error field is too large) then plasma deceleration is triggered, which has the effect of deviating the plasma into the unstable region of parameter space once the no-wall stability limit is exceeded.

The faster the rotation is ramped, the less time the plasma spends in the vicinity of the error-field resonance, and, hence, the less time the mode has in which to grow to a dangerous amplitude.

As can be seen from Fig. 3, the extent of the unstable region of parameter space decreases with increasing plasma dissipation, making it more difficult for error-field induced

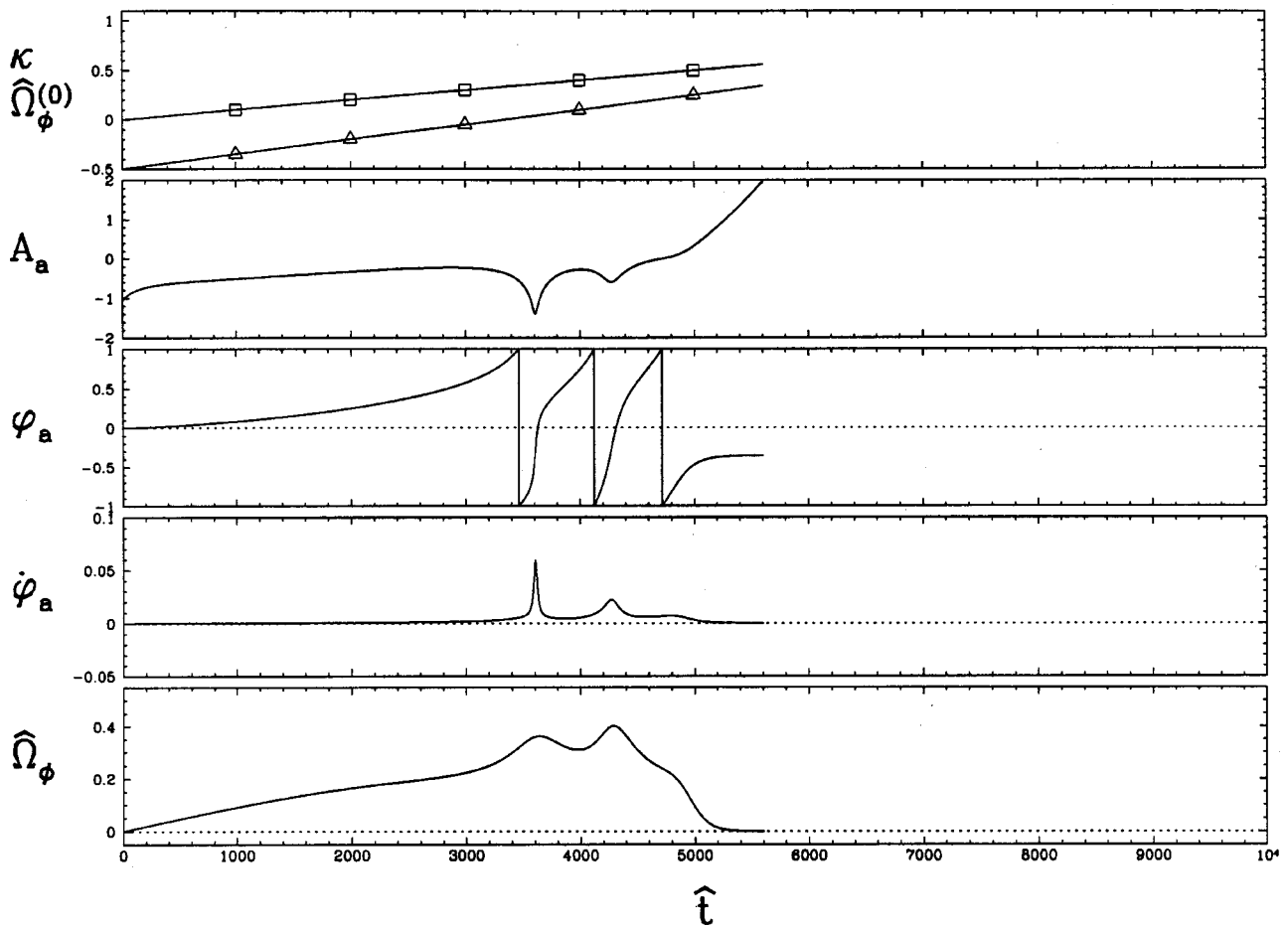


FIG. 10. Simulation of a DIII-D NBI heating ramp in which the equilibrium plasma rotation and stability parameters increase linearly. The other parameters are $\Psi_c = 0.10$, $\nu_* = 0.66$, $S_* = 100$, $m = 3$, and $r_w = 1.2a$. The five panels show (1) the stability parameter, κ (triangles), and the equilibrium rotation parameter, $\hat{\Omega}_\phi^{(0)}$ (squares), (2) the mode amplitude parameter, $A_a = \log_{10}(|\Psi_a|)$, (3) the mode phase, $\varphi_a = \arg(\Psi_a)$ (units of π), (4) the mode phase velocity, $\dot{\varphi}_a = d\varphi/d\hat{t}$, (5) the plasma rotation parameter, $\hat{\Omega}_\phi$.

plasma deceleration to deviate the plasma into the unstable region.

D. Estimate of critical parameters for DIII-D plasmas

Let us estimate the values of the various normalized quantities appearing in our mode evolution equations for a typical DIII-D plasma. The major parameters of the DIII-D device are as follows:^{16,17} $R_0 = 1.67$ m, $a = 0.67$ m, $r_w = 1.2a$, $\tau_w = 6$ ms, $B_\phi = 2.1$ T, and $n_e = 2 \times 10^{19}$ m⁻³, where n_e is the electron number density. Our reference plasma discharge is characterized by $q(0) = 1.3$ and $q(a) = 2.9$ (the low edge- q value is an artifact of the cylindrical nature of our model). For the $m = 3$, $n = 1$ mode, we find $c = 1.7 \times 10^{-2}$, $d = 0.17$, $\kappa = 0.33$, $d_c = 0.25$, and $s(a) = 2$. It follows that $\Omega_0/2\pi \sim 14$ kHz, $\Omega_c/2\pi \sim 6$ kHz, $\nu_* \sim 0.2\chi$ (m/s²), and $S_* \sim 90$. Here, χ is the edge momentum diffusivity. Since χ typically lies between 1 and 5 m/s² in DIII-D plasmas, the dissipation parameter ν_* lies in the range 0.1 to 1. Note that our estimate for Ω_c is a little high, but in the right ballpark. All times are normalized by $t_0 = 1/\Omega_0 \sim 10$ μ s, and all mode amplitudes by $b_0 = B_\phi \sqrt{cd}(\tau_A \Omega_0) = 3 \times 10^{-3}$ T. It can be

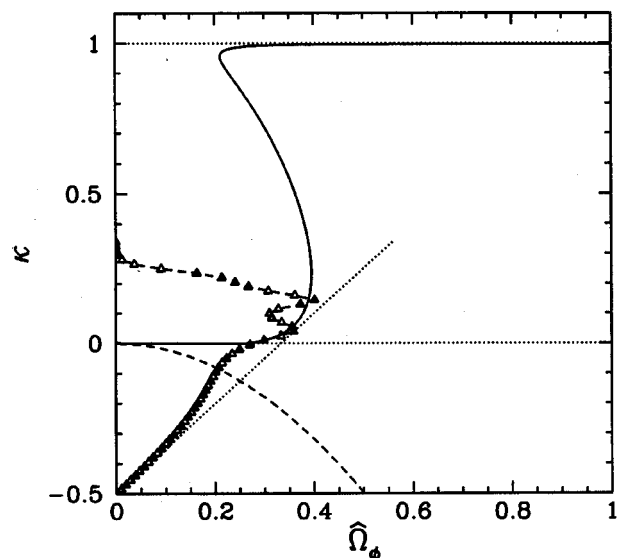


FIG. 11. The trajectory (triangles) of the simulation shown in Fig. 10 plotted at equal time intervals in $\hat{\Omega}_\phi - \kappa$ space. The dashed curve shows the error-field resonance. The solid curve shows the stability boundary for the RWM.

seen that the parameter values used in the previous simulations are fairly appropriate to DIII-D plasmas. We estimate that the typical RWM amplitude needed to trigger plasma deceleration in DIII-D (unity in normalized units) is about 30 G, whereas the critical error-field strength above which access to the wall stabilized region is denied (between 0.02 and 0.1 in normalized units) lies in the range 1–3 G. These estimates accord well with experimental observations. Note, however, that the above estimates are fairly inexact due to the difficulty in representing highly shaped, single-null, DIII-D plasmas using a cylindrical model.

V. SUMMARY

In Sec. II, the previously published¹⁵ Fitzpatrick–Aydemir dispersion relation for the resistive wall mode (RWM) in a large-aspect ratio, rotating, viscous tokamak plasma is discussed. At low plasma dissipation, there are two stable regions in the parameter space of plasma rotation versus plasma stability. The first stable region is restricted to relatively low plasma rotation rates, and lies well below the perfect-wall stability boundary. The second stable region only exists above a critical plasma rotation rate, which depends on the dissipation, and extends almost to the perfect-wall boundary. These two regions are separated by a band of instability. The thickness and extent of this band both decrease as the plasma dissipation increases. At high plasma dissipation, the band of instability disappears altogether, and the first and second stable regions merge.

In Sec. III, a set of evolution equations for the RWM is derived which take into account the nonlinear deceleration of the plasma rotation generated by mode interaction with both the resistive wall and a static error field. This is achieved by combining the Fitzpatrick–Aydemir dispersion relation with a plasma equation of rotational motion.

In Sec. IV, a number of simulations are performed with the above mentioned RWM evolution equations in order to study access to the wall stabilized region in DIII-D. We generally expect a DIII-D plasma to start off well below the no-wall stability boundary, and to access the wall stabilized region via an NBI induced ramp in the plasma β and rotation. Unfortunately, the plasma must cross an error-field resonance and (possibly) an unstable region of parameter space in order to achieve this goal. The simulations presented in this paper indicate that this is possible provided that the error-field amplitude is not too large. If the error field is too large then the RWM grows to a sufficiently high amplitude to trigger plasma deceleration, which effectively blocks entry into the wall stabilized region.

Note that, in general, the error-field resonance *does not* correspond to a RWM marginal stability curve in parameter

space. The reason for this is that, in general, the RWM possesses a nonzero real frequency at marginal stability. Of course, the error-field resonance is associated with the response of the plasma to a zero frequency perturbation.

The estimated critical plasma rotation frequency in DIII-D needed to stabilize the RWM is about 6 kHz. The estimated RWM amplitude required to trigger plasma deceleration is about 30 G. Finally, the estimated error-field amplitude needed to prevent access to the wall stabilized region is about 2 G. These estimates are in broad agreement with experimental observations.

ACKNOWLEDGMENTS

The author would like to thank Anders Bondeson (Chalmers University of Technology), Gerry Navratil, Mike Mauel, Allan Boozer, Andrea Garofalo (Columbia University), and Rob La Haye (General Atomics) for helpful discussions during the preparation of this paper.

This research was funded by the U.S. Department of Energy under Contract No. DE-FG05-96ER-54346.

¹C. Kessel, J. Manickam, G. Rewoldt, and W. M. Tang, Phys. Rev. Lett. **72**, 1212 (1994).

²E. A. Lazarus, G. A. Navratil, C. M. Greenfield *et al.*, Phys. Rev. Lett. **77**, 2714 (1996).

³The conventional definition of this parameter is $\beta = 2\mu_0 \langle p \rangle / \langle B^2 \rangle$, where $\langle \dots \rangle$ denotes a volume average, p is the plasma pressure, and B is the magnetic field strength.

⁴A. Bondeson, M. Benda, M. Persson, and M. S. Chu, Nucl. Fusion **37**, 1419 (1997).

⁵J. P. Goedbloed, D. Pfirsch, and H. Tasso, Nucl. Fusion **12**, 649 (1972).

⁶T. S. Taylor, E. J. Strait, L. L. Lao *et al.*, Phys. Plasmas **2**, 2390 (1995).

⁷M. Okabayashi, N. Pomphrey, J. Manickam *et al.*, Nucl. Fusion **36**, 1167 (1996).

⁸A. M. Garofalo, E. Eisner, T. H. Ivers *et al.*, Nucl. Fusion **38**, 1029 (1998).

⁹A. Bondeson and D. J. Ward, Phys. Rev. Lett. **72**, 2709 (1994).

¹⁰R. Betti and J. P. Freidberg, Phys. Rev. Lett. **74**, 2949 (1995).

¹¹A. B. Mikhailovskii and B. N. Kushinov, Plasma Phys. Rep. **21**, 802 (1995).

¹²A. Bondeson and M. S. Chu, Phys. Plasmas **3**, 3013 (1996).

¹³R. Betti, Phys. Plasmas **5**, 3615 (1998).

¹⁴D. Gregoratto, A. Bondeson, M. S. Chu, and A. M. Garofalo, Plasma Phys. Controlled Fusion **43**, 1425 (2001).

¹⁵R. Fitzpatrick and A. Y. Aydemir, Nucl. Fusion **16**, 11 (1996).

¹⁶A. M. Garofalo, A. D. Turnbull, M. E. Austin *et al.*, Phys. Rev. Lett. **82**, 3811 (1999).

¹⁷A. M. Garofalo, A. D. Turnbull, E. J. Strait *et al.*, Phys. Plasmas **6**, 1893 (1999).

¹⁸A. H. Boozer, Phys. Plasmas **2**, 4521 (1995).

¹⁹J. M. Finn, Phys. Plasmas **2**, 3782 (1995).

²⁰C. G. Gimblett and R. J. Hastie, Phys. Plasmas **7**, 258 (2000).

²¹A. H. Boozer, Phys. Rev. Lett. **86**, 5059 (2001).

²²A. Bondeson and M. Persson, Nucl. Fusion **28**, 1887 (1988).

²³R. Fitzpatrick, Phys. Plasmas **6**, 1168 (1999).

²⁴R. Fitzpatrick, Nucl. Fusion **33**, 1049 (1993).